[Skip to main content]

Last updated on None.

This ATBD was developed in the context of the ESA-funded CIMR DEVALGO study (2022-2024) (contract 4000137493).

ESA is not responsible in any way for the content of this document.

MR L2 Soil Moisture ATBD

ts

nent describes the algorithm theoretical basis for the Soil Moisture product.

act

ithm Theoretical Basis Document (ATBD) presents the theoretical basis for the Imaging Microwave Radiometer (CIMR) soil moisture (SM) retrieval algorithm. o, the forthcoming CIMR mission carries on the legacy of successful L-band uch as SMOS, SMAP, and Aquarius.

sed algorithm for the retrieval of SM is based on the simultaneous retrieval of ure and vegetation properties. It builds on the tau-omega radiative transfer heritage of the SMOS-IC algorithm and the SMAP Multi-Temporal Dual Channel but evolves to reduce dependencies on ancillary information by exploiting CIMR ral characteristics and daily revisit. It utilizes both H-polarized and V-polarized temperature (TB) observations at the L-band frequency (~1.4 GHz) to estimate CIMR bands, L-band has the highest sensitivity to SM but also the coarsest olution.

to disaggregate L-band using C/X bands at a higher spatial resolution, leading moisture products: the first is based on the inversion of L-band-only TBs at its lution (~60 km, Hydroclimatological), and the second involves the inversion of L- enhanced spatial resolution (~10 to 25 km, Hydrometeorological). In addition to ire, the algorithm also delivers a second product: the vegetation optical depth , derived from L, C, X and Ku bands, that represents the degree of attenuation of vaves through the canopy. This microwave vegetation parameter is an ecological hat correlates well with diverse vegetation attributes such as water content and

cable and reference documents

licable and reference documents

cument
Donlon. Copernicus Imaging Microwave Radiometer (CIMR) Mission uirements Document v5.0, available [here]

nyms

ced Microwave Scanning Radiometer-EOS

ced Scatterometer

nicus Imaging Microwave Radiometer

hannel Algorithm

Area Scalable Earth

ean Space Agency

and Agriculture Organization

ational Geosphere-Biosphere Programme

urface Temperature

rate Resolution Imaging Spectroradiometer

Temporal Dual Channel Algorithm

al Aeronautics and Space Administration

alized Difference Vegetation Index

ive Transfer Model

Frequency Interference

oisture

oisture Active Passive

oisture and Ocean Salinity

e Radar Topography Mission

e Water Fraction

ness Temperature

inated Universal Time

ation Optical Depth

ation Water Content

itions used in this ATBD

ws a glossary, or list of definitions

s Temperature

rightness Temperature is the temperature of a surface as seen by a passive wave sensor. It is a measure of the amount of energy emitted by a surface. It is expressed in Kelvin.

us Imaging Microwave Radiometer

opernicus Imaging Microwave Radiometer is a Microwave Radiometer which is planned by ESA in 2029.

area projection grid definition based on a Lambert Azimuthal projection and a
4 datum. Defined in [Brodzik *et al.*, 2012].

nnel Algorithm

thm used in SMAP to retrieve simultaneously two parameters (soil moisture and tion optical depth).

onal Geosphere-Biosphere Programme

ternational Geosphere-Biosphere Programme land cover classification defines tems surface classifications based on vegetation characteristics and land use.

nporal Dual Channel Algorithm

lulti-Temporal Dual Channel Algorithm (MT-DCA) is an evolution of DCA that nformation from multiple SMAP overpasses to improve retrieval performance.

ture

oisture is defined as the water held in the spaces between soil particles, and it is ly expressed as a ratio, either by volume-to-volume ratio (m^3/m^3) or by weight.

ture Active Passive

MAP (Soil Moisture Active Passive) mission is a NASA satellite mission launched in hat uses both active and passive microwave sensors to measure soil moisture.

ture and Ocean Salinity

MOS (Soil Moisture and Ocean Salinity) mission, launched in 2009 by the ean Space Agency, is dedicated to making global observations of soil moisture nd and salinity over oceans using a passive microwave sensor.

on Optical Depth

ation optical depth (VOD) is a parameter that characterizes the extinction effects o vegetation, including attenuation and scattering, on microwave radiations gating through the vegetation canopy. It is related almost linearly to the ation water content and indirectly to vegetation water status and biomass

duction, purpose and scope

se of this Algorithm Theoretical Baseline Document (ATBD) is to present the that will be used in the Copernicus Imaging Microwave Radiometer (CIMR) derive Soil Moisture (SM) products from the brightness temperatures (TB) from the CIMR radiometer. Initially, the historical background of passive remote sensing for soil moisture is provided, along with the justification for the orithm. As detailed in the Level-2 product definition section, the output product in data structured on a geographical grid (EAE2, Equal Area Cylindrical .

dure for extracting soil moisture information from CIMR TB observations employs nega model, widely used in the passive microwave soil moisture community. The algorithm is based on the SMOS-IC algorithm for SMOS and the Multi-Temporal nnel Algorithm for SMAP. This design has been adapted to the particular tics of CIMR.

Soil Moisture retrieval algorithm takes into consideration the impact of a layer covering the soil. This layer absorves partially the emission of the soil and e overall radiative flux its own emission. By accounting for this absorption, the generates a complementary product known as the vegetation optical depth, spatial resolution depending on the CIMR band. Utilizing the L-band brightness re measurements enables accurate estimation of soil moisture, while C and X-used to sharpen L-band TB spatial resolution. The algorithm provides the soil roducts at two distinct spatial resolutions: a hydroclimatological scale based on of L-band TB (~60 km) and an enhanced hydrometeorological scale based on f L-band TB at enhanced spatial resolution (~10 to 25 km).

seline Algorithm Definition” section, the forward model and CIMR retrieval are presented, including a flow diagram that outlines all the steps involved in al of L-band soil moisture and vegetation optical depth. Finally, the Algorithm Output Data Definition section outlines all the necessary input and output data orithm.

ground and justification of selected ithm

ure is a crucial part of the Earth's water cycle and it has been monitored for l purposes, water supply management, climate forecasting, forest fire prediction atmosphere interactions [Dorigo *et al.*, 2017]. Soil moisture is defined as the water held in the soil, and relates to precipitation, evaporation, and plant uptake ne *et al.*, 2010]. Changes in soil moisture can have substantial impacts on l productivity, forest and the general ecosystem health.

ure was identified as an essential climate variable (ECV) by the Global Climate System (GCOS), due to its importance for understanding and monitoring the Earth's climate system. Soil moisture estimation over large areas and long challenging due to its spatial and temporal variability. However, remote sensing es have revolutionized the ability to measure soil moisture over large areas, facilitated numerous applications in several fields, including hydrology, , and climate modeling [Entekhabi *et al.*, 2010].

and timely measurements of soil moisture are crucial for improving our ding of the Earth's climate system and its associated processes [Vereecken *et al.*, instance, monitoring soil moisture can help predict droughts, floods, and which can save lives and reduce economic losses. It can also help optimize water ent and irrigation practices, leading to increased agricultural productivity and Furthermore, soil moisture data can improve weather and climate forecasting by the accuracy of precipitation estimates and address priority questions on climate identifying patterns and trends that affect the Earth's climate [Koster *et al.*,

mote sensing of soil moisture is a technique used to estimate soil moisture ver large areas and at high temporal resolution [Kerr *et al.*, 2001]. Passive sensors are used to measure the natural thermal radiation emitted from the soil ne intensity of this radiation varies depending on the dielectric properties and re of the target medium, which in the case of the near surface soil layer, is by the amount of moisture present in the near surface soil layer. The low frequencies at L-band (~1 GHz) have additional benefits for soil moisture ent: the atmosphere is almost entirely transparent, making it possible to sense ure regardless of weather conditions and signals from the underlying soil can be d through thin vegetation layers.

cal heritage

of passive remote sensing for soil moisture estimation dates back to the 1960s. period , researchers began to look at ways of using microwaves to measure ent in the soil. The first successful experiments used a single-channel microwave to measure the brightness temperature of the surface of the Earth. This data used to calculate the soil moisture content [Schmugge, 1983]. In the 1970s and number of channels of the radiometer was increased and more sophisticated re developed to better measure soil moisture. This included the use of multiple bands and polarimetric techniques to better characterize the soil moisture.

oth Nimbus-7 and the short-lived Seasat were launched, each equipped with the Multichannel Microwave Radiometer (SMMR) instrument. SMMR, a 10-channel operating at frequencies between 6.6 and 37 GHz, achieved spatial resolutions om approximately 150 km to 30 km. It acted as a precursor to the Advanced Scanning Radiometer (AMSR) and its subsequent version, AMSR2 [Njoku and Li, SR was launched in 2002 and it has been used for soil moisture estimation as ther applications such as sea ice concentration and snow depth. It is the or of the Advanced Microwave Scanning Radiometer 2 (AMSR2), launched in ard the GCOM-W1 satellite [Wu *et al.*, 2020].

mote sensing for soil moisture estimation has gone through several iterations, ces in hardware and software technology allowing for more accurate and precise ents. Today, passive remote sensing is one of the most widely used methods for ure estimation, with satellites, aircraft, and ground-based instruments all g to its knowledge.

ns from the CIMR (Copernicus Imaging Microwave Radiometer) mission will offer continuity to the brightness temperature and soil moisture measurements rom ESA's SMOS (Soil Moisture Ocean Salinity) [Kerr *et al.*, 2001] and NASA's l Moisture Active Passive) [Entekhabi *et al.*, 2010] and Aquarius missions. This also extends to the data from AMSR and AMSR2 instruments.

al approach

Rayleigh-Jeans approximation. When the microwave sensor orbits above the observed TB includes energy from the soil (attenuated by the vegetation), and , downwelling atmospheric emission and cosmic background emission reflected ace and attenuated by vegetation, and the upwelling atmospheric emission (Fig. mosphere transmissivity (τ_{atm}) is approximately equal to 1, and the cosmic d temperature (T_{sky}) is around 2.7 K.

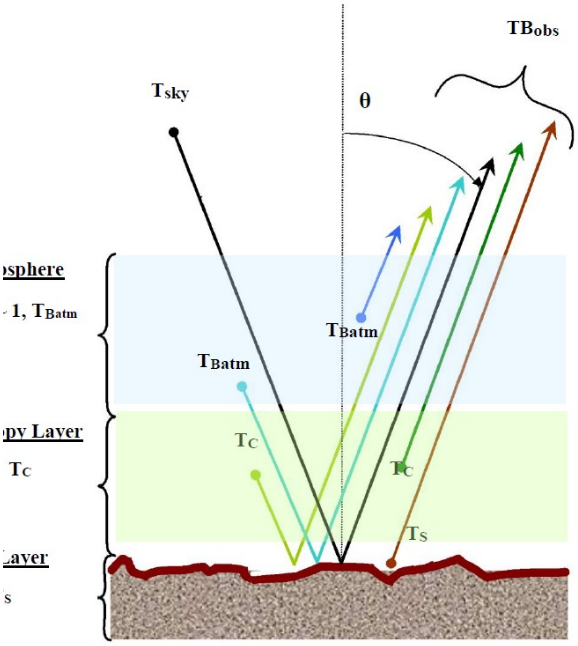

ntributions to the Top Of Atmosphere (TOA) brigthness temperature [from SMOS 12 and SMAP ATBD, Figure 2]

ss of obtaining soil moisture information from CIMR TB observations involves tau-omega model, which is commonly employed in the passive microwave soil ommunity. This model takes into account the impact of a layer of vegetation ne soil, which affects the emission of the soil and adds to the overall radiative flux nission. When working with L band frequencies, it is generally assumed that the within the vegetation is negligible, so the vegetation can be considered primarily rbing layer.

ation of selected algorithm

ion, we justify the selection of our proposed algorithm, which is founded on the algorithm for SMOS {cite:p}wigneron2007; fernandez-moran2017 and the Dual lgorithm for SMAP {cite:p}Chaubell2022; KONINGS2017. This algorithm makes h H-polarized and V-polarized TB observations to estimate soil moisture and optical depth or vegetation opacity, τ at L-band. The choice of this band is to its ability to penetrate deeper into vegetation, providing more accurate ents. Thus, in the presence of dense biomass, the transmissivity decays in a lower L-band (1.4 GHz), as compared to higher frequencies: C-band (6 GHz), and X-GHz) frequencies, also sensitive to soil moisture but to a lesser extent. Various luding vegetation biomass, cloud liquid water, soil moisture, surface roughness, rated water vapour, influence the TB differently across each CIMR band, as in the referenced figure (Fig. 2). Considering that the highest sensitivity is t the L-band, this provides insight into why both SMOS and SMAP utilize L-band global soil moisture estimation under a range of vegetation conditions. It must that measuring soil moisture at L-band has the added benefit of capturing emission from deeper within the soil, typically around 5 cm, whereas C- and X-ssions primarily originate from a thinner layer. This is feasible due to the between soil moisture and soil permittivity and the connection between soil y and soil emissivity. For that, the passive microwave remote sensing community oped numerous soil dielectric models in recent decades, which, despite their , commonly utilize soil moisture, soil texture, and frequency. Well-known nclude Dobson, Wang & Schmugge, and Mironov. For this project, we opted for ov model due to its flexibility and strong performance when utilizing the soil's ntage as the sole ancillary data [Mialon *et al.*, 2015].

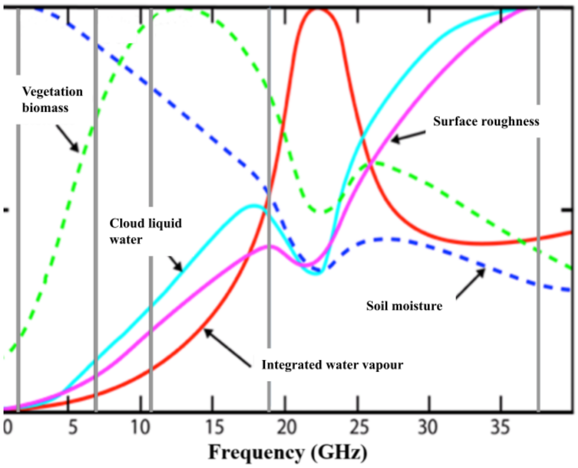

sitivity of TB to different factors across CIMR bands (adapted from [Kerr, 1996])

tant to note that at L-band, another parameter of interest, τ, can be retrieved. τ the attenuation of L-band microwave radiation by the vegetation canopy. While is typically studied using optical or infrared frequencies, the longer wavelengths sensors allow radiation to penetrate the canopy more effectively. As a result, τ ıked to a variety of vegetation attributes, such as forest height, vegetation water content, sap flow, and leaf fall. Furthermore, some vegetation indices, like rea Index (LAI) and the Normalized Difference Vegetation Index (NDVI), can also ed with τ. Notably, several studies have emphasized the substantial influence of ıess on the retrieved τ values at both local and regional scales [Grant *et al.*, 2016, -Moran *et al.*, 2017].

-2 product definition

Table 1 L2-product

r	Description	Units	Dimensions
	Longitude [0°, 360°]	*deg East*	$(xdim_{grid}, ydim_{grid})$
	Latitude [90°S, 90°N]	*deg North*	$(xdim_{grid}, ydim_{grid})$
	seconds since YYYY-MM-DD 00:00:00 UTC	*seconds*	$(xdim_{grid}, ydim_{grid})$
	L1B Brightness Temp at L-band	*K*	$(xdim_{grid}, ydim_{grid})$
	L1B Enhanced Temp at L-band	*K*	$(xdim_{grid}, ydim_{grid})$
	Soil Moisture	m^3/m^3	$(xdim_{grid}, ydim_{grid})$
	Enhanced Soil Moisture	m^3/m^3	$(xdim_{grid}, ydim_{grid})$
	Veg Optical Depth	-	$(xdim_{grid}, ydim_{grid})$
	Enhanced Veg Optical Depth	-	$(xdim_{grid}, ydim_{grid})$
	Veg single scattering albedo	-	$(xdim_{grid}, ydim_{grid})$
index	Row index in EASE2 grid	-	$(xdim_{grid}, ydim_{grid})$
column	Column index in EASE2 grid	-	$(xdim_{grid}, ydim_{grid})$
E	RMSE between measured and modeled TB	*K*	$(xdim_{grid}, ydim_{grid})$
ИSE	RMSE between enhanced and modeled TB	*K*	$(xdim_{grid}, ydim_{grid})$
ʝs	RFI, proximity to water body, etc.	*8-bits flag*	$(xdim_{grid}, ydim_{grid})$
ȷ	Product quality flag	*n/a*	$(xdim_{grid}, ydim_{grid})$

esearch in the passive microwave soil moisture field has led to the development us soil moisture retrievals that can be applied to CIMR TB data. The ESA's SMOS rrently operates an aperture synthesis L-band radiometer that produces TB data incidence angles for identical ground locations. The core SMOS retrieval utilizes the tau-omega model and takes advantage of SMOS's ability to capture cidence angles for soil moisture estimation. SMAP retrievals, on the other hand, ised on the tau-omega model but employ the constant incidence angle TB data y the SMAP radiometer, an approach more similar to the forthcoming CIMR onsequently, we propose a retrieval algorithm that incorporates elements from MOS-IC and the SMAP multi-channel algorithm.

ve radiometer's primary function is to detect the inherent thermal radiation that from a surface. Under the Rayleigh-Jeans approximation, the intensity of the emission at microwave frequencies is directly proportional to the product of the emperature and emissivity, commonly referred to as the brightness temperature

microwave sensor orbits the Earth, several factors contribute to the observed TB. ıde the soil's emitted energy (attenuated by overlying vegetation), the emission etation itself, downwelling atmospheric emission and cosmic background (reflected by the surface and attenuated by vegetation), and upwelling ic emission.

se of L band frequencies, the atmosphere is virtually transparent, with an ic transmissivity (τ_atm) of approximately 1. The cosmic background, or Tsky, is K. Additionally, atmospheric emission is minimal.

d Model

val of soil moisture from CIMR surface TB observations relies on a widely l approximation to the radiative transfer equation referred to as the tau-omega ich, in this case, is referred to as the forward model. In tau-omega, a soil layer vegetation attenuates the soil's emission while contributing its own emission to radiative flux. Given that scattering within vegetation is generally negligible at L iencies, the vegetation can be predominantly treated as an absorbing layer [Kerr , O'Neill *et al.*, 2020]. Thus, TB can be expressed as follows:

$$e_p exp(-\tau_p \sec\theta) + T_c(1-\omega_p)[1-\exp(-\tau_p \sec\theta)][1+r_p\exp(-\tau_p \sec\theta)] \quad (1)$$

subscript p refers to polarization (V or H), Ts denotes the soil temperature and for the canopy temperature, τ_p represents the nadir vegetation opacity, ω_p ds to the vegetation single scattering albedo (ω), and rp is the soil reflectivity of rface. The reflectivity is connected to the emissivity (ep) through the relation ep It must be noted that ω_p will be treated here as an effective parameter [Kurum,

to Beer's law, the overlying canopy layer's transmissivity or vegetation n factor , γ, is given by γ = exp(-τ_p sec θ). Equation (1) assumes that vegetation attering and reflection at the vegetation-air interface are negligible.

ughness is modeled as r_p = r*_p exp (-H_R), where H_R parameterizes the f the roughness effects, r*_p stands for the reflectivity of a plane surface. Nadir opacity is related to the total vegetation water content (VWC, in kg/m2) by τ_p with the coefficient bp dependent on vegetation type and microwave frequency zation) {cite:p}Van De Griend2004.

e reflectance rp is characterized by the Fresnel equations, which detail the an electromagnetic wave when interacting with a smooth surface. When an gnetic wave encounters a surface that separates two media with different roperties (e.g., air and soil), part of the wave's energy is reflected at the surface, transmitted through it. The Fresnel equations are used to calculate the amount eflected based on the incident angle of the wave and the dielectric properties of ed media. For horizontal polarization, the wave's electric field aligns parallel to ing surface and perpendicular to the propagation direction. In contrast, for larization, the electric field of the wave has a component perpendicular to the quations (2)(3) show the Fresnel equations for both horizontal and vertical ns.

$$r_H(\theta) = \left| \frac{\cos\theta - \sqrt{\epsilon - \sin^2\theta}}{\cos\theta + \sqrt{\epsilon - \sin^2\theta}} \right|^2 \quad (2)$$

$$| \epsilon \cos\theta + \sqrt{\epsilon - \sin^2\theta} |$$

epresents the CIMR incidence angle, while ε denotes the soil layer's complex onstant.

tant to note that an increase in soil moisture is accompanied by a proportional the soil dielectric constant (ε). For instance, liquid water has a dielectric constant ile dry soil possesses a dielectric constant of 5. Furthermore, it should be ged that a low dielectric constant is not uniquely indicative of dry soil conditions. , regardless of water content, exhibits a dielectric constant similar to that of dry equently, a freeze/thaw flag is required to resolve this ambiguity. Since TB is al to emissivity for a given surface soil temperature, TB decreases as soil ncreases. In the CIMR algorithm, ε is expressed as a function of SM, soil clay d soil temperature using the model developed by Mironov [Mironov *et al.*, 2012].

onship between soil moisture and soil dielectric constant (and consequently emissivity and brightness temperature) establishes the basis for passive remote soil moisture. With CIMR observations of TB and information on T_s and T_c, _p from ancillary sources, soil moisture (SM) and vegetation optical depth (VOD) trieved. The procedure for this retrieval is detailed in the following section, Method'.

'al Method

plementing the soil moisture retrieval, a preliminary step is to perform a water ection to the brightness temperature data for cases where a significant of the grid cells contain open water. As it is well known, brightness temperature ably decrease when the water fraction increases [Ulaby and Long, 2014], leading estimation of the retrieved SM values [Ye *et al.*, 2015] and inducing artificial cles of VOD [Bousquet *et al.*, 2021]. It is therefore important to correct the CIMR temperatures for the presence of water, to the extent feasible, prior to using puts to the Level-2 Soil Moisture retrieval. This correction needs to be performed CIMR Hydrology Target mask ([RD-1] MRD-854), as part of the optimal on or re-sampling process (in the CIMR RGB toolbox). The hydrology target mask information from both permanent and transitory water surfaces that shall be with the surface water seasonality information provided by the CIMR Surface tion (SWF) product as well as ancillary information.

dure to acquire soil moisture (SM) and vegetation optical depth (VOD, also τ) requires the minimization of the cost function F, as shown in (4). The method e F is the Trust Region Reflective (TRR) algorithm [Branch *et al.*, 1999].

$$F(SM,\tau) = \frac{(TB_p^{obs} - TB_p)^2}{\sigma(TB)^2} + \sum_{i=1}^{2} \frac{(P_i^{ini} - P_i)^2}{\sigma(P_i)^2} \quad (4)$$

term TB_p^{obs} refers to the observed value, while $\sigma(TB)$ denotes the standard ssociated with the brightness temperature measurements (a constant value of 1 Additionally, $TB_p(\theta)$ is the brightness temperature calculated using Equation uation also incorporates a regularization term, where P_i $(i = 1, 2)$ represents the parameter value (SM, VOD), P_i^{ini} $(i = 1, 2)$ is an a priori estimate of the P_i, and $\sigma(P_i)$ is the standard deviation associated with this estimate.

onstant value of $0.2m^3/m^3$ is assumed for SM and $\sigma(SM)$, while the value of t to the average yearly value (calculated from previous runs). The $\sigma(\tau_{NAD})$ is as shown in Equation (5).

$$\sigma(\tau_{NAD}) = \min(0.1 + 0.3 \cdot \tau_{NAD}, 0.3) \quad (5)$$

Level-1b re-sampling approach

Level-2 Soil Moisture retrieval algorithm will provide two soil moisture products: ased on the inversion of L-band only TBs at its native resolution (<60 km, atological), the second one based on the inversion of L-band at an enhanced olution (~10 to 25 km Hydrometeorological). The enhanced L-band targets an ean spatial resolution of 15-km and is based on sharpening techniques that C-band and X-band channels (Zhang et al., in prep. 2023).

3 illustrates the Level-1b resampling approach starting with a Backus-Gilbert or ter Image Reconstruction analysis applied at L-band with footprints matched to d channel in swath geometry (at CIMR RGB Toolbox). The objective of this first ptimize L-band reconstruction to provide the highest possible spatial resolution

-bands to estimate an equivalent 15 km L-band. The effective resolution of the TB_L_E products will be evaluated and compared (e.g. as in [Long et al., 2023]). Level-2 Processor are initially being planned to be provided in C-band channel metry although the convenience of using gridded products (including generation :) needs to be assessed at a later phase during the project. The third step is the on an Earth-based map projection grid. CIMR Level-2 Soil Moisture products ective spatial resolution of <60 km (L-band only) and ~15 km (after sharpening bands) are planned to be projected on a 9 km EASE2 grid. The CIMR radiometer scanning and its high degree of oversampling provides flexibility in resampling supporting the use of a finer grid (posting resolution) than the TB effective [Long et al., 2023]. At L-band, CIMR TB measurements are collected with an spacing of approximately 8 km, while there is an overlap of 29 % in the along-tion (no spacing). The proposed 9 km gridding resolution is thus initially selected e as much information as possible. Note that the use of the same gridding for the two products will facilitate their direct comparison and algorithm development at this stage of the project, but the use of an EASE2 grid with a km (then multiples thereof), e.g. 9 km and 36 km as shown in Fig. Fig. 3 will also red upon characterization of the tradeoff between noise and spatial resolution gridded images.

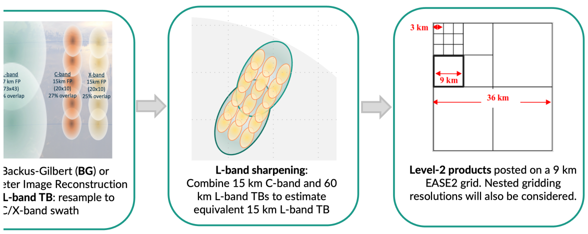

nceptual flow of Level-1b resampling to exploit CIMR oversampling and nested solution and achieve global hydroclimatology and hydrometeorology soil moisture onal requirements of 60 and 15 km spatial resolution daily.

:hm Assumptions and Simplifications

algorithm incorporates several simplifications, which are detailed below.

scending and descending satellite passes, it is assumed that the air, vegetation, urface soil are in thermal equilibrium, given that the canopy temperature (Tc) can imated to the soil temperature (Ts) [Fernandez-Moran et al., 2017, Hornbuckle nd, 2005]. In this context, we can represent both temperatures with a single mperature (Teff).

soil roughness parameterization, the formulation used is simplified to represent ness with a single parameter, H, derived from the full formulation proposed by Choudhury [Wang and Choudhury, 1981]. For simplification purposes, both soil and vegetation scattering albedo are considered time invariant, despite their ing on a global scale.

rder radiative transfer model, also known as the tau-omega model, is utilized by stimate soil moisture. This model is a zero-order solution of the microwave ransfer equations, which neglects multiple reflections within the vegetation ome studies have attempted to address this limitation by utilizing higher-order ansfer models, such as the Two Stream Emission Model (2S-EM) [Schwank et al., he approach proposed by Feldman [Feldman et al., 2018]. Feldman's approach o quantify higher order scattering through the First Order Scattering Model (First 1), introducing an additional term for multiple scattering (Ω1) alongside the er scattering term (ω), using a ray-tracing method.

2 end to end algorithm functional flow diagram

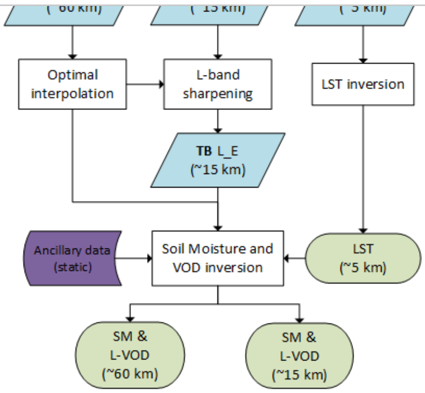

ctional flow diagram of Level-2 Soil moisture and VOD retrieval algorithm.

onal description of each Algorithm step

cessing of input TB

ssing algorithm primarily relies on the CIMR L1B TB product that is calibrated, l and undergoes several corrections, such as atmospheric effects, Faraday d RFI effects. L, C, and X-bands are used as inputs to the Soil Moisture and VOD At each of these frequencies, fore- and aft-look TB data are merged and for the presence of standing water. L-band undergoes an optimal interpolation econstruction step and is resampled to C-band channel swath geometry (at the ox). This product, TB_L, is directly used as input to the Level-2 retrieval algorithm the SM and L-VOD at coarse resolution (<60km). TB_L is also combined with C ds into an enhanced-resolution product TB_L_E, that is used as input to the Level- to obtain SM and L-VOD at an enhanced spatial resolution (~15km).

ds are processed independently to obtain the effective land surface temperature d as input in the Soil Moisture and VOD retrieval step, together with other static ata. This temperature can be initially derived from CIMR Ka band using the linear formulation of Holmes [Holmes *et al.*, 2009], although the use of the CIMR LST ECMWF will also be considered.

surface quality and surface conditions

ata will be employed to help to determine whether masks are in effect for strong y, urban, snow/ice, frozen soil.

ta

data for the model consists of two primary parameters. The first is the Level 1b Temperature (L1B TB), which is observed by CIMR at L, C, and X-bands, covering ontal and vertical polarizations. This data represents a full swath or swath section nsions *(Nscans, Npos)* in a 2D array format. The second parameter, TB_err, the error associated with the Brightness Temperature. This error information is ized with the same dimensions, *(Nscans, Npos)*. This information is showed in

data

outputs include key parameters such as soil moisture and vegetation optical coarse and an enhanced resolution. The output data is presented in a 9 km . Additional information like brightness temperature, geographical data, albedo, flags supplement these outputs. Data flags enable users to examine (a) the nditions of a grid cell, (b) the potential impact of RFI, and (c) the quality of soil stimate when retrieval is attempted.

ls can be found in IODD.

data

f Land Surface Temperature will be included as ancillary data: the one estimated Ka/Ku bands and the one from ECMWF. This will allow for some flexibility in the l validation phase of the algorithm prototype.

within a given CIMR pixel. The data used for these computations are derived IGBP classification as identified in the study conducted by Fernandez-Moran -Moran *et al.*, 2017]. In Table Values of ω and H, different values of ω and H are rding to land cover type. Based on these criteria, static global maps of ω and H produced as part of the ancillary dataset.

Table 2 Values of ω and H

IS IGBP land fication	SMAP MTDCA ω	SMAP DCA ω	CIMR ω	SMOS-IC H	CIMR H
reen Needleleaf Forests	0.07	0.07	0.06	0.30	0.40
reen Broadleaf Forests	0.08	0.07	0.06	0.30	0.40
uous Needleleaf Forests	0.06	0.07	0.06	0.30	0.40
uous Broadleaf Forests	0.07	0.07	0.06	0.30	0.40
d Forests	0.07	0.07	0.06	0.30	0.40
d Shrublands	0.08	0.08	0.10	0.27	0.27
Shrublands	0.06	0.07	0.08	0.17	0.10
ly Savannas	0.08	0.08	0.06	0.30	0.40
nas	0.07	0.10	0.10	0.23	0.23
lands	0.06	0.07	0.10	0.12	0.50
anent Wetlands	0.16	0.10	0.10	0.19	0.19
ands - Average	0.10	0.06	0.12	0.17	0.40
and Built-up Lands	0.08	0.08	0.10	0.21	0.21
land/Natural Vegetation ics	0.09	0.10	0.12	0.22	0.50
and Ice	0.11	0.00	0.10	0.12	0.12
n	0.02	0.00	0.12	0.02	0.10

re, a CIMR Hydrology Target mask, applied in Level-2 data processing, provides a olution and covers both permanent and transitory inland water surfaces. The porates data from the MERIT Hydro [Yamazaki *et al.*, 2019] and the Global Lakes nds Database [Lehner and Döll, 2004], and it will be updated up to four times account for potential seasonal changes. Its calculation involves a previous of the Surface Water Fraction (SWF) data.

flag incorporate information about RFI, proximity to water body, urban, rozen soil, precipitation, medium and strong topographic effects.

datasets that complement the ancillary information are the clay fraction (from IGBP Land Cover type Classification (from MODIS) and the Digital Elevation ained from the Shuttle Radar Topography Mission (SRTM) [Jarvis *et al.*, 2006, *l.*, 2008].

ithm Input and Output Data Definition D)

data

Table 3 Input Data

r	Description	Shape/Amount
	L1B Brightness Temperature at L, C and X-bands (both H and V polarization)	*Full swath or swath section (Nscans, Npos)*
	Random radiometric uncertainty of the channels	*Full swath or swath section (Nscans, Npos)*

t data

r	Description	Units	Dimensions
	Longitude [0°, 360°]	*deg East*	$(xdim_{grid}, ydim_{grid})$
	Latitude [90°S, 90°N]	*deg North*	$(xdim_{grid}, ydim_{grid})$
	seconds since YYYY-MM-DD 00:00:00 UTC	*seconds*	$(xdim_{grid}, ydim_{grid})$
	L1B Brightness Temperature at L-band	*K*	$(xdim_{grid}, ydim_{grid})$
	L1B Enhanced Brightness Temperature at L-band	*K*	$(xdim_{grid}, ydim_{grid})$
	Soil Moisture	m^3/m^3	$(xdim_{grid}, ydim_{grid})$
	Enhanced Soil Moisture	m^3/m^3	$(xdim_{grid}, ydim_{grid})$
	Vegetation Optical Depth	-	$(xdim_{grid}, ydim_{grid})$
	Enhanced Vegetation Optical Depth	-	$(xdim_{grid}, ydim_{grid})$
	Vegetation single scattering albedo	-	$(xdim_{grid}, ydim_{grid})$
index	Row index in EASE2 grid	-	$(xdim_{grid}, ydim_{grid})$
olumn	Column index in EASE2 grid	-	$(xdim_{grid}, ydim_{grid})$
E	RMSE between measured and modeled TB	*K*	$(xdim_{grid}, ydim_{grid})$
ISE	RMSE between enhanced and modeled TB	*K*	$(xdim_{grid}, ydim_{grid})$
js	Flag to indicate difficult inversion situations	*8-bit flag*	$(xdim_{grid}, ydim_{grid})$
j	Product quality flag	*n/a*	$(xdim_{grid}, ydim_{grid})$

ry data

Table 5 Ancillary data

r	Description	Shape/Amount
F	CIMR Surface Water Fraction	*(Nscans, Npos)*
	CIMR Land Surface Temperature	*(Nscans, Npos)*
	Land Surface Temperature (from ECMWF)	*(Nscans, Npos)*
e	Clay fraction (from FAO)	*(Nscans, Npos)*
	IGBP Land Cover type Classification (from MODIS)	*(17, Nscans, Npos)*
	Vegetation single scattering albedo (from SMOS-IC)	*(Nscans, Npos)*
	Surface roughness information (from SMOS-IC)	*(Nscans, Npos)*
	Digital Elevation Model	*(Nscans, Npos)*
_mask	CIMR Hydrology Target mask ([RD-1, MRD-854])	*(Nscans, Npos)*

ithm Performance Assessment (Version D)

ences

I. J. Brodzik, B. Billingsley, T. Haran, B. Raup, and M. H. Savoie. EASE-Grid 2.0: cremental but Significant Improvements for Earth-Gridded Data Sets. *ISPRS ternational Journal of Geo-Information*, 1(1):32 – 45, 2012. oi:10.3390/ijgi1010032.

/. Dorigo, W. Wagner, C. Albergel, and others. Esa cci soil moisture for improved arth system understanding: state-of-the art and future directions. *Remote ensing of Environment*, 203:185–215, 2017. doi:10.1016/j.rse.2017.07.001.

I. Seneviratne, T. Corti, E. L. Davin, and others. Investigating soil moisture–imate interactions in a changing climate: a review. *Earth-Science Reviews*, 99:125–61, 2010. doi:10.1016/j.earscirev.2010.02.004.

Skip to main content

map) mission. Proceedings of the IEEE, 98:704–716, 2010. oi:10.1109/JPROC.2010.2043918.

. Vereecken, J. A. Huisman, H. Bogena, and others. On the value of soil moisture easurements in vadose zone hydrology: a review. *Water Resources Research*, 008. doi:10.1029/2008WR006829.

. D. Koster, P. A. Dirmeyer, Z. Guo, and others. Regions of strong coupling etween soil moisture and precipitation. *Science*, 305:1138–1140, 2004. oi:10.1126/science.1100217.

ann H Kerr, Philippe Waldteufel, Jean-Pierre Wigneron, Jean Martinuzzi, Jordi ont, and Michel Berger. Soil moisture retrieval from space: the soil moisture and cean salinity (smos) mission. *IEEE Transactions on Geoscience and Remote ensing*, 39(8):1729–1735, 2001.

homas J. Schmugge. Remote sensing of soil moisture: recent advances. *IEEE ransactions on Geoscience and Remote Sensing*, GE-21(3):336–344, 1983. oi:10.1109/TGRS.1983.350563.

G. Njoku and Li Li. Retrieval of land surface parameters using passive microwave easurements at 6-18 ghz. *IEEE Transactions on Geoscience and Remote Sensing*, 7(1):79–93, 1999. doi:10.1109/36.739125.

anghai Wu, Yu Wang, Cheng-Zhi Zou, Rui Li, Shi Liu, Guosheng Liu, and Yunfei u. A fundamental climate data record derived from amsr-e, mwri, and amsr2. *IEEE ransactions on Geoscience and Remote Sensing*, 58(8):5450–5461, 2020. oi:10.1109/TGRS.2020.2966055.

rnaud Mialon, Philippe Richaume, Delphine Leroux, Simone Bircher, Ahmad Al tar, Thierry Pellarin, Jean-Pierre Wigneron, and Yann H. Kerr. Comparison of obson and mironov dielectric models in the smos soil moisture retrieval gorithm. *IEEE Transactions on Geoscience and Remote Sensing*, 53(6):3084 – 3094, 015. Cited by: 53. doi:10.1109/TGRS.2014.2368585.

H. Kerr. Optimal choice for miras frequencies: scientific requirements. Technical eport, CESBIO, Toulouse, 1996. Project MMS MIRAS N° CCM3.

P. Grant, J.P. Wigneron, R.A.M. De Jeu, H. Lawrence, A. Mialon, P. Richaume, . Al Bitar, M. Drusch, M.J.E. van Marle, Y. Kerr, and others. Comparison of smos nd amsr-e vegetation optical depth to four modis-based vegetation indices. *emote Sensing of Environment*, 172:87–100, 2016. doi:.

. Fernandez-Moran, J.-P. Wigneron, G. De Lannoy, E. Lopez-Baeza, M. Parrens, . Mialon, A. Mahmoodi, A. Al-Yaari, S. Bircher, A. Al Bitar, and others. A new alibration of the effective scattering albedo and soil roughness parameters in the mos sm retrieval algorithm. *International Journal of Applied Earth Observation nd Geoinformation*, 62:27–38, 2017. doi:10.1016/j.jag.2017.05.013.

. Kerr, P. Waldteufel, P. Richaume, I. Davenport, P. Ferrazoli, and J.-P. Wigneron. mos level 2 processor soil moisture algorithm theoretical basis document (atbd). echnical Report SO-TN-ESL-SM-GS-0001, CESBIO, SM-ESL (CBSA), Toulouse, rance, 2006.

eggy O'Neill, Rajat Bindlish, Steven Chan, Julian Chaubell, Eni Njoku, and Tom ckson. Soil moisture active passive (smap) algorithm theoretical basis document: vel 2 & 3 soil moisture (passive) data products. Technical Report JPL D-66480, ASA Goddard Space Flight Center and Jet Propulsion Laboratory, California stitute of Technology, Greenbelt, MD and Pasadena, CA and Beltsville, MD, ugust 2020.

lehmet Kurum. Quantifying scattering albedo in microwave emission of egetated terrain. *Remote Sensing of Environment*, 129:66–74, 2013. URL: ttps://www.sciencedirect.com/science/article/pii/S0034425712004099, oi:https://doi.org/10.1016/j.rse.2012.10.021.

. Mironov, Y. Kerr, S. Member, J. Wigneron, and S. Member. Temperature- and exture-dependent dielectric model for moist soils at 1.4 ghz. *IEEE Geosci. Remote ens. Lett.*, 10:1–5, 2012.

awwaz T. Ulaby and David G. Long. *Microwave Radar and Radiometric Remote ensing*. University of Michigan Press, 2014. doi:10.3998/0472119356.

Ye, J P Walker, J Guerschman, D Ryu, and R J Gurney. Standing water effect on oil moisture retrieval from L-band passive microwave observations. *Remote Sens. nviron.*, 169:232–242, 2015. URL: ttps://www.sciencedirect.com/science/article/pii/S0034425715301012, oi:https://doi.org/10.1016/j.rse.2015.08.013.

mma Bousquet, Arnaud Mialon, Nemesio Rodriguez-Fernandez, Catherine rigent, Fabien H Wagner, and Yann H Kerr. Influence of surface water variations n VOD and biomass estimates from passive microwave sensors. *Remote Sens. nviron.*, 257:112345, 2021. URL: ttps://www.sciencedirect.com/science/article/pii/S0034425721000638, oi:https://doi.org/10.1016/j.rse.2021.112345.

l. A. Branch, T. F. Coleman, and Y. Li. A subspace, interior, and conjugate gradient ethod for large-scale bound-constrained minimization problems. *SIAM Journal n Scientific Computing*, 21(1):1–23, 1999.

ightness temperature image products. IEEE Transactions on Geoscience and
emote Sensing, 57(7):4151–4163, 2019. doi:10.1109/TGRS.2018.2889427.

avid G Long, Mary J Brodzik, and Molly Hardman. Evaluating the effective esolution of enhanced resolution SMAP brightness temperature image products. *ront. Remote Sens.*, 2023. URL: ttps://www.frontiersin.org/articles/10.3389/frsen.2023.1073765, oi:10.3389/frsen.2023.1073765.

K. Hornbuckle and A.W. England. Diurnal variation of vertical temperature radients within a field of maize: implications for satellite microwave radiometry. *EE Geoscience and Remote Sensing Letters*, 2(1):74–77, 2005. oi:10.1109/LGRS.2004.841370.

R. Wang and B.J. Choudhury. Remote sensing of soil moisture content over bare eld at 1.4 ghz frequency. *Journal of Geophysical Research*, 86:5277–5282, 1981.

l. Schwank, R. Naderpour, and C. Mätzler. "tau-omega"- and two-stream nission models used for passive l-band retrievals: application to close-range easurements over a forest. *Remote Sensing*, 10(12):1868, 2018. oi:10.3390/rs10121868.

ndrew F. Feldman, Ruzbeh Akbar, and Dara Entekhabi. Characterization of gher-order scattering from vegetation with smap measurements. *Remote ensing of Environment*, 219:324–338, 2018. URL: ttps://www.sciencedirect.com/science/article/pii/S0034425718304760, oi:10.1016/j.rse.2018.10.022.

R. H. Holmes, R. A. M. De Jeu, M. Owe, and A. J. Dolman. Land surface emperature from ka band (37 ghz) passive microwave observations. *J. Geophys. es. Atmos.*, 2009.

. Yamazaki, D. Ikeshima, J. Sosa, P.D. Bates, G.H. Allen, and T.M. Pavelsky. Merit ydro: a high-resolution global hydrography map based on latest topography ataset. *Water Resources Research*, 55(6):5053–5073, 2019.

Lehner and P. Döll. Development and validation of a global database of lakes, eservoirs and wetlands. *Journal of Hydrology*, 296(1-4):1–22, 2004.

. Jarvis, H. Reuter, A. Nelson, and E. Guevara. Hole-filled seamless srtm data v3. echnical Report, 2006.

rnaud Mialon, Laurent Coret, Yann H. Kerr, FranÇois Secherre, and Jean-Pierre Vigneron. Flagging the topographic impact on the smos signal. *IEEE Transactions n Geoscience and Remote Sensing*, 46(3):689–694, 2008. oi:10.1109/TGRS.2007.914788.

ean-Pierre Wigneron, Yann Kerr, Philippe Waldteufel, Kontar Saleh, Maria-Jose scorihuela, Philippe Richaume, Paolo Ferrazzoli, Patricia de Rosnay, Robert urney, Jean-Christophe Calvet, and others. L-band microwave emission of the iosphere (l-meb) model: description and calibration against experimental data ets over crop fields. *Remote Sensing of Environment*, 107:639–655, 2007.

Fernandez-Moran, A. Al-Yaari, A. Mialon, A. Mahmoodi, A. Al Bitar, . De Lannoy, N. Rodriguez-Fernandez, E. Lopez-Baeza, Y. Kerr, and J.-P. Vigneron. Smos-ic: an alternative smos soil moisture and vegetation optical epth product. *Remote Sensing*, 9:457, 2017. doi:10.3390/rs9050457.

teven K. Chan, Rajat Bindlish, Peggy E. O'Neill, Eni Njoku, Thomas Jackson, ndreas Colliander, Fan Chen, Mariko Burgin, R. Scott Dunbar, Jeffrey Piepmeier, nd others. Development and assessment of the smap enhanced passive soil oisture product. *Remote Sensing of Environment*, 204:931–941, 2018. oi:10.1016/j.rse.2017.08.025.

ulian Chaubell, Simon Yueh, R. Scott Dunbar, Andreas Colliander, Dara Entekhabi, teven K. Chan, Fan Chen, Xiaolan Xu, Rajat Bindlish, Peggy Oaneill, Jun Asanuma, aron A. Berg, David D. Bosch, Todd Caldwell, Michael H. Cosh, Chandra Holifield ollins, Karsten H. Jensen, Jose Martinez-Fernandez, Mark Seyfried, Patrick J. tarks, Zhongbo Su, Marc Thibeault, and Jeffrey P. Walker. Regularized dual-hannel algorithm for the retrieval of soil moisture and vegetation optical depth om smap measurements. *IEEE Journal of Selected Topics in Applied Earth bservations and Remote Sensing*, 15:102 – 114, 2022. Cited by: 6; All Open ccess, Gold Open Access. doi:10.1109/JSTARS.2021.3123932.

lexandra G. Konings, Maria Piles, Narendra Das, and Dara Entekhabi. L-band egetation optical depth and effective scattering albedo estimation from smap. *emote Sensing of Environment*, 198:460–470, 2017. oi:https://doi.org/10.1016/j.rse.2017.06.037.

driaan A. Van De Griend and Jean-Pierre Wigneron. The b-factor as a function of equency and canopy type at h-polarization. *IEEE Transactions on Geoscience and emote Sensing*, 42(4):786–794, 2004. Cited by: 132. oi:10.1109/TGRS.2003.821889.